Volcanic eruption forecasts from accelerating rates of drumbeat long-period earthquakes

Citation for published version:
Bell, AF, Naylor, M, Hernandez, S, Main, IG, Gaunt, HE, Mothes, P & Ruiz, M 2018, 'Volcanic eruption forecasts from accelerating rates of drumbeat long-period earthquakes' Geophysical Research Letters, vol 45, no. 3, pp. 1339-1348. DOI: 10.1002/2017GL076429

Digital Object Identifier (DOI):
10.1002/2017GL076429

Link:
Link to publication record in Edinburgh Research Explorer

Document Version:
Peer reviewed version

Published In:
Geophysical Research Letters

Volcanic eruption forecasts from accelerating rates of drumbeat long-period earthquakes

Andrew F. Bell [1], Mark Naylor[1], Stephen Hernandez[2], Ian G. Main[1], H. Elizabeth Gaunt[2], Patricia Mothes[2], and Mario Ruiz[2]

[1]School of GeoSciences, University of Edinburgh, Edinburgh, U.K.

[2]Instituto Geofísico, Escuela Politécnica Nacional, Quito, Ecuador

Corresponding author: Andrew Bell (a.bell@ed.ac.uk)

Key Points:

- Power-law acceleration in rates of long period earthquakes observed before large explosive eruption at Tungurahua volcano, Ecuador
- Earthquake source characteristics indicate repeated quasi-periodic activation of single source driven by accelerated loading
- New Bayesian gamma point process methodology applied to analyze dataset and provide probabilistic eruption forecasts

Abstract

Accelerating rates of quasi-periodic 'drumbeat' long period earthquakes (LPs) are commonly reported before eruptions at andesite and dacite volcanoes, and promise insights into the nature of fundamental pre-eruptive processes and improved eruption forecasts. Here we apply a new Bayesian MCMC gamma point process methodology to investigate an exceptionally well-developed sequence of drumbeat LPs preceding a recent large vulcanian explosion at Tungurahua volcano, Ecuador. For more than 24 hours, LP rates increased according to the inverse power-law trend predicted by material failure theory, and with a retrospectively forecast failure time that agrees with the eruption onset within error. LPs resulted from repeated activation of a single characteristic source driven by accelerating loading, rather than a distributed failure process, showing that similar precursory trends can emerge from quite different underlying physics. Nevertheless such sequences have clear potential for improving forecasts of eruptions at Tungurahua and analogous volcanoes.

1. **Introduction**

Accelerating rates of geophysical signals, such as seismicity (Kilburn & Voight, 1998; De La Cruz-Reyna & Reyes-Dávila, 2001; Neuberg et al., 2000; Ramos et al., 1999; Salvage & Neuberg, 2016; Voight, 1988; Voight & Cornelius, 1991) or ground deformation (McGuire & Kilburn, 1997), have been reported before a wide range of eruption styles. Such sequences evolve over timescales of minutes (Linde et al., 1993) to years (Robertson & Kilburn, 2016), and provide an opportunity for both improved understanding of the physical processes that control the approach to eruption, and more reliable, quantitative, eruption forecasts (Bell et al., 2013; Boué et al., 2015, 2016).

Here we apply a new Bayesian gamma point process model to analyse LP earthquakes preceding the July 2013 eruption at Tungurahua. We find rates increase over 24 hours according to Eq. (2), but with quasi-periodic inter-event times. Earthquake amplitudes also increase towards the eruption, despite the decreasing inter-event times. 'Pseudo-prospective' forecasts illustrate the predictability of the process, including the effect of catalogue completeness close to eruption. First we summarize the earthquake data and statistical methods used. We then apply the new model in retrospective and simulated forecasting modes to evaluate model fit and parameter values, and determine likely forecasting performance. We then discuss the implications of our findings for understanding of volcanic processes, LP source mechanisms, and eruption forecasting.

1.1. Material failure and volcanic earthquakes

Similarities between accelerating pre-eruptive trends and those associated with material failure phenomena (Main, 1999; Vasseur et al., 2017) mean that they are often analysed within this conceptual framework (Kilburn, 2003; Main, 1999; Voight, 1988). Failure of all or part of the volcanic system (in response to elevated magma and gas pressure) is associated with a fundamental empirical relation between the acceleration in a geophysical precursor Ω (such as strain or number of earthquakes) and its rate:

$$\frac{d^2\Omega}{dt^2} = K\left(\frac{d\Omega}{dt}\right)^{\alpha} \qquad (1)$$

where α and K are constants. In the common case that $\alpha > 1$, solutions to Equation (1) take the form of an inverse power-law increase in the mean rate of precursory signals with time (Kilburn, 2003):

$$\frac{d\Omega}{dt} = k\left(t_f - t\right)^{-p} \qquad (2)$$

where the power-law exponent, $p = 1/(\alpha - 1)$ describes the non-linearity of the acceleration, and k reflects the absolute amplitude (Bell & Kilburn, 2013). Equation (2) involves a singularity at a finite time, t_f, corresponding to an infinite precursor rate, realization of a system-wide fracture and the percolation threshold, and often equated to the initiation of the eruption process (Voight, 1988).

The material failure paradigm has most commonly been considered in the context of high frequency (5-15 Hz) volcano-tectonic earthquakes (VTs) (Bell & Kilburn, 2012; Kilburn & Voight, 1998). VTs result from brittle stick-slip and fracture events within the edifice, and are prevalent at volcanoes re-awakening after long repose intervals (Kilburn & Voight, 1998), or at systems strongly influenced by edifice deformation (Bell & Kilburn, 2012; Collombet, 2003) or tectonic processes (Sigmundsson et al., 2014). The temporal occurrence of VTs is generally consistent with an inhomogeneous Poisson or clustered point process (Bell et al., 2011). Their magnitudes follow a Gutenberg-Richter distribution (Roberts et al., 2015), and sources are commonly distributed across many locations in the deforming system. As such, these characteristics share many fundamental similarities with generic failure phenomena (Kilburn, 2012; Main, 1999; Vasseur et al., 2017)

VTs are less common before eruptions at open-system andesitic and dacitic volcanoes, providing limited forecasting information. Instead, low frequency (1-5 Hz), long period earthquakes ('LPs') dominate seismicity before explosive or effusive events (McNutt, 2005). Their waveform properties involve emergent onsets and extended (often harmonic) coda, and require a strong resonance or scattering effect (Chouet & Matoza, 2013). LPs are potentially excited by a diverse range of source mechanisms, including hydrothermal fluid movement (Lipovsky & Dunham, 2015), brittle magma failure (De Angelis & Henton, 2011; Lavallée et al., 2008; Neuberg et al., 2006; Tuffen et al., 2008), incremental plug ascent (Iverson et al., 2006; Johnson et al., 2008), slow rupture of a poorly consolidated shallow edifice (Bean et al., 2013), or gas depressurization (Gil-Cruz & Chouet, 1997). For LPs at Tungurahua, suggested source mechanisms include gas depressurization (Molina, 2004), magma stick-slip or failure (Neuberg et al., 2018), and coupled magma ascent and gas depressurization (Bell et al., 2017). The statistical properties of LPs often include a restricted range or 'characteristic' distribution of magnitudes (Bell et al., 2017), repeating waveforms indicating multiple reactivation of a small number of source locations (Green & Neuberg, 2006), and periodic (anti-clustered) inter-event times, sometimes referred to as 'drumbeat' earthquakes (Bell et al., 2017; Iverson et al., 2006; White et al., 1998). Although accelerating rates of LPs have been reported before eruptions at several volcanoes (Boué et al., 2015; Neuberg et al., 2000; Salvage & Neuberg, 2016), it is not clear if these characteristics are consistent with the physics of a material failure process, and how such data and their patterns may be best used for forecasting.

1.2. Tungurahua volcano and precursors to the 14 July 2013 explosion

Tungurahua is an active andesitic stratovolcano in the Eastern Cordillera of the Ecuadorian Andes (Arellano et al., 2008), monitored by the network of the Instituto Geofísico of the Escuela Politécnica Nacional (IGEPN). The ongoing eruption began in 1999, involving episodes of vulcanian and strombolian activity, some with large paroxysmal explosions, interspersed by periods of quiescence of a few months (Hidalgo et al., 2015). Seismicity is dominated by low frequency signals, with few VT or hybrid earthquakes. Eruptive episodes are commonly preceded by a few hours or days of elevated rates of LPs. At

11:47 UTC on 14 July 2013, Tungurahua experienced the largest paroxysmal explosion of the current eruption, with the highest amplitude acoustic energy recorded at Tungurahua, accompanied by a large gas plume, and sending ash to a height of 8.3 km above the vent (Hall et al., 2015). The eruptive products primarily consisted of very low permeability 'plug' material, with relatively little juvenile pumaceous content (Hall et al., 2015).

2. Data and methods

2.1. Monitoring data

Seismic data associated with the eruption were recorded by the monitoring network of the IGEPN. The seismicity was best recorded at the nearest 1 Hz short-period vertical component seismometer located at station 'RETU', at 3900 m elevation (Bell et al., 2017). Primary seismic data manipulation was undertaken using the Obspy python library (Krischer et al., 2015). The highly similar earthquake waveforms indicates closely located sources, meaning that the amplitude recorded at RETU is a reasonable approximation of relative earthquake energy release. Peak amplitudes and 15 second RMS amplitudes yield similar results. Data from RETU were manually picked to provide an earthquake catalogue for several days before and after the paroxysmal explosion, and used to provide five minute relative seismic amplitude (RSAM). 960 events were picked in the 24 hours before the explosion, of which 427 were recorded in the unlocated IGEPN catalogue for Tungurahua. None of the earthquakes were of sufficiently high amplitude to be detected on the broader IGEPN seismic network, and so are no locations are available, although typical horizontal and vertical location uncertainties for LP earthquakes at Tungurahua are on the order of a few km (Bell et al., 2017). As the earthquakes are only well-recorded at RETU, they are likely to be located at shallow levels in the edifice, and most probably in or close to the conduit.

2.2. Periodicity

We define periodicity as the ratio between the mean and standard deviation of the inter-event times (Bell et al., 2017). For earthquakes that are randomly distributed in time (i.e. a Poisson process), with average rate λ, the inter-event times follow an exponential distribution with mean $\mu = 1/\lambda$ and variance $\sigma^2 = 1/\lambda^2$. Therefore, the periodicity, $\mu/\sigma = 1$. The periodicity is equivalent to the coefficient of variation for the earthquake rate. The variance of inter-event times for earthquakes that are clustered in time will be relatively high, giving values of periodicity less than 1. The variance of highly periodic (anti-clustered) earthquakes will be relatively small, resulting in periodicity values greater than 1. For a gamma distribution the periodicity is $\sqrt{\gamma}$ (see supporting information).

2.3. Gamma point process models

For quasi-periodic earthquake processes, Poisson process models will incorrectly estimate parameters and their uncertainties. We model earthquake occurrence times as an inhomogeneous gamma process (Barbieri et al., 2001), with a mean rate evolving according to Equation (2). A gamma process is a generalized form of Poisson process for quasi-periodic data, and has been used to analyse biomedical data, such as neuron spiking (Barbieri et al., 2001) and heartbeats (Barbieri et al., 2005). For clustered data, the gamma distribution has previously been shown to be an emergent property of the superposition of independent earthquakes and triggered earthquakes (Touati et al., 2009) or a non-homogeneous Poisson process of independent earthquakes with an underlying rate change (Shcherbakov et al., 2005). However to our knowledge the gamma distribution has not previously been applied to quasi-periodic volcanic earthquake point process data. We use a Bayesian approach to estimate model parameters (Boué et al., 2015), but here applying Markov Chain Monte Carlo (MCMC) to the point process model likelihood function rather than binned event rates. MCMC is implemented through PyMC3 (Salvatier et al., 2016).

3. Results

3.1. Precursors to eruption

Average LP rates, amplitudes, and RSAM increased systematically in the 24 hr lead up to the 14 July explosion (Fig. 1a; Fig. 3, Fig. S1). Individual LP earthquakes have peak frequencies of 2-3 Hz (Fig. 1b-d), an emergent onset, and coda of 20-30 seconds duration. Many earthquake waveforms are highly similar, indicating the repeated activation of fixed-location sources (Fig. 2a and b). Cross-correlation analysis, using a two-stage clustering method (Bell et al., 2017; Green & Neuberg, 2006; Rodgers et al., 2013) with cross-correlation thresholds of 0.7 and 0.8, finds only one dominant family of earthquakes with highly correlated waveforms, suggesting repeated activation of a single source location, but where the source progressively evolves through time (either due to a small change in location, or small change in source mechanism; Fig. 2a-c). Earthquake inter-event times are quasi-periodic, approximating a gamma distribution when the systematic rate increase is accounted for (Fig. 2d), meaning that they are not independent. Average inter-event times decrease from greater than 10 minutes early in the sequence to less than 10 s close to the explosion. At 200 minutes before the explosion, inter-event times decrease to equal to or less than the coda duration, so individual waveforms merge into continuous (non-harmonic) tremor (Fig. 1d), as seen at other volcanoes including Redoubt and Soufriere Hills (Hotovec et al., 2013; Neuberg et al., 2000). The merger results in masking of individual earthquakes, and hence an incomplete earthquake catalogue close to the eruption, despite efforts to pick earthquakes in the frequency domain, and using a template matching approach. Earthquake amplitudes have a restricted range of values that approximate a lognormal distribution (inconsistent with a power-law Gutenberg-Richter distribution of amplitudes). Despite hours of accelerating LP rates and amplitudes, the final onset of the paroxysmal explosion was effectively instantaneous (Fig. 1d).

3.2. Bayesian MCMC application of FFM to quasi-periodic data

The observed increases in LP earthquake rates, amplitudes, and RSAM towards the explosion all closely follow the trend described by Equation (2) (Fig. 3). Retrospective modelling (i.e. with known fixed eruption time) finds distinctly different values of p for the different metrics (Fig. 3). The mean of the posterior distribution of p is 1.05 for earthquake rate, (excluding incomplete data within 200 minutes of the eruption time), whereas it takes values of 0.23 and 0.38 for amplitudes and RSAM, respectively. Retrospective ‘forecasts’ (estimating the eruption time alongside other model parameters) also closely approximate the data (Fig 3 a-c) and highlight the marked difference between p for different data types, but show greater variance in the posterior distributions due to the covariance between p and t_f when the eruption time is not fixed. For both cases, observed earthquake rates fall below model predictions closer than 200 minutes before the eruption whereas average earthquake amplitudes and RSAM more closely follow equation (2) up to the eruption onset (Fig 3 b & c).

3.3. Retrospective forecasts and posterior parameter distributions

Repeated retrospective forecasts reveal the evolution of parameter posterior distributions, including the failure time, as the sequence progresses (Fig. 4). The means of posterior distributions for t_f (Fig. 4a) and p (Fig. 4b) based on earthquake times are stable until 90% of the sequence is complete. The uncertainty in these parameters (including the eruption time) decrease towards eruption as depicted by the width of the 5% and 95% credibility intervals, and the indicative posterior probability density distributions. The mean t_f is one hour later than the actual eruption time, though within the estimated uncertainty. The eruption occurred whilst earthquake rates, amplitudes, and RSAM were still increasing (at the time of onset, the mean inter-event times were 8-9 s). After 90% of the sequence, catalogue incompleteness becomes important and results in an increasingly biased (late) estimate. The degree of periodicity increases systematically through the sequence (Fig. 4c), and likely increases even further in the final 10% of the sequence, but is partly masked by incompleteness. Similar analysis based on earthquake amplitudes and RSAM show much greater variance in model parameters until very close to the eruption, as a result of lower values of p and greater non-linearity of the acceleration. Close to the eruption, these metrics continue to increase according to a power-law (Fig. 3 b & c), and so provide more reliable information about eruption timing.

Synthetic datasets can reproduce many of the characteristics of the real data (Fig. S3), and their analysis provides further constraints on the nature of pre-eruptive sequences. Waveform superposition results in an apparent power-law increase in earthquake amplitude at inter-event times less than the earthquake coda duration, even for synthetic sequences generated with constant input amplitude. Synthetic simulations show that the apparent power-law trends and low exponent values for amplitude and RSAM are most easily explained by an underlying linear increase in amplitude with time (Fig. S4). These properties are therefore emergent consequences of the power-law increase in earthquake rate, a linear increase in the 'true' earthquake size, and waveform superposition, and so may not hold much physical significance in themselves. Residual discrepancies between simulations and observations suggest that the acceleration in earthquake rate slows slightly in the final hour before the eruption, though incompleteness means that it is not possible to resolve this effect in the real data. Simulations also show that forecasting error (i.e. the variance of the posterior distribution of t_f) decreases with increasing periodicity (e.g. Fig. S5), and so eruption forecasts based on quasi-periodic drumbeat signals are expected to be more precise than those for equivalent sequences with Poisson or clustered in inter-event times.

4. Discussion

Quasi-periodic inter-event times, a systematically increasing restricted range of amplitudes, and highly-similar waveforms suggest that LPs in this sequence involve repeated energy release from a single source location, most likely within or close to the conduit. Short inter-event times close to the eruption imply rapid (<8-9 s) source re-activation is required, including loading (e.g. shear stress or gas pressure increase) and renewal (e.g. fault or magma healing, magma ascent). These characteristics are not consistent with a process underpinned by material failure distributed through a large volume, even though the observed power-law increase in mean earthquake rate with $p \approx 1$ are the same as those predicted by that model for VT earthquakes at reawakening volcanoes (Kilburn, 2003). Rather, we suggest that these similarities result as emergent properties of different complex, non-linear physical systems.

LP amplitudes are reported to decrease with increasing earthquake rate before some explosions at Soufriere Hills (Neuberg et al., 2000) and Redoubt (Buurman et al., 2013). Such behaviour might indicate that progressive weakening of the seismic source controls the approach to eruption, but is inconsistent with observations here. Increasing amplitudes with increasing earthquake rates have been reported for precursory sequences before large tectonic earthquakes (Bouchon et al., 2011) and landslides (Poli, 2017), and attributed to increasing slip or size of a repeatedly failing asperity within a zone of accelerating aseismic slip. For this model to translate to the pre-eruptive sequence at Tungurahua would require accelerating aseismic ascent of the magma column to drive repeated failure of a growing local asperity such as a patch undergoing frictional stick-slip (Iverson et al., 2006) or shear failure of magma (Neuberg et al., 2006; Tuffen & Dingwell, 2005), whilst maintaining co-located sources to produce similar earthquake waveforms and sufficiently high gas pressure to drive the ensuing explosion. The short inter-event times close to failure are difficult to explain with a magma failure and healing model (Chouet & Matoza, 2013; Tuffen et al., 2003), unless new magma is continually ascending into a seismogenic window (Neuberg et al., 2006). Existing models for LP generation at Tungurahua suggest that the excitation mechanism might involve local gas depressurization (Bell et al., 2017; Molina, 2004). A 'two-phase' model (Bell et al., 2017; Holland et al., 2011), where excitation results from gas flux and depressurization, but earthquake timing is determined by a transient breach of a low permeability barrier through shear failure near the column margins driven by magma ascent, allows greater independence between inter-event times and amplitudes. This model might provide an explanation for the broader range of LP signals observed at Tungurahua (Bell et al., 2017), and an alternative interpretation of the processes underlying this sequence.

In either scenario, accelerating earthquake rates and increasing amplitudes and RSAM are likely to be driven by steadily accelerating magma ascent and high gas pressures, implying both magma flow from depth and gas exsolution from supersaturated melt (Lensky et al., 2008). The eruption onset occurs slightly before the predicted failure time, when the system reaches some hidden critical threshold. The highly explosive, gas-driven vulcanian nature of the eruption suggests that this is when the gas pressure exceeds the failure strength of the plug, or the inter-event time reduces to either the finite duration of the source mechanism or recovery time. The different characteristics of trends in LP earthquake rates, amplitudes, and RSAM suggest the most informative forecasts of explosion timing would be initially based on LP occurrence times, with additional information close to the eruption provided by RSAM and earthquake amplitudes. Future work will see these different metrics combined into an integrated Bayesian forecasting tool.

5. Conclusions

This work outlines a new approach for reliable and informative retrospective analyses of pre-eruptive LP seismicity, and verifiable and testable Bayesian forecasts. When applied to the July 2013 eruption, the methods reveal a remarkable sequence, resembling a theoretical ideal to a degree not reported before. The powerful paroxysmal explosion, involving relatively little juvenile magma, is indicative of an eruption driven by high gas pressures and a very low permeability barrier to gas ascent. Unusually, the resulting quasi-periodic oscillating system, likely involving coupled incremental magma ascent and increasing gas pressure, remained stable until a late stage. The methods offer quantitative, probabilistic forecasts of the timing of explosions when pre-eruptive seismicity follow a quasi-periodic power-law acceleration. Understanding of when and how these conditions might arise, and how to reliably identify them in noisy data, is key for improved eruption forecasting in future.

Acknowledgments

A.F.B. was partly funded by a Carnegie trust research incentive grant. We thank S. De Angelis and an anonymous review for insightful and constructive comments that helped improve the manuscript. We also thank the staff of the IGEPN for their considerable efforts in maintaining the monitoring network on Tungurahua volcano. Seismic data for Tungurahua is curated by the IGEPN and available on request from http://www.igepn.edu.ec/solicitud-de-datos

References

De Angelis, S., & Henton, S. M. (2011). On the feasibility of magma fracture within volcanic conduits: Constraints from earthquake data and empirical modelling of magma viscosity. *Geophysical Research Letters*, *38*(19), n/a-n/a. https://doi.org/10.1029/2011GL049297

Arellano, S. R., Hall, M. L., Samaniego, P., Le Pennec, J.-L., Ruiz, A., Molina, I., & Yepes, H. A. (2008). Degassing patterns of Tungurahua volcano (Ecuador) during the 1999-2006 eruptive period, inferred from remote spectroscopic measurements of SO2 emissions. *Journal of Volcanology and Geothermal Research*, *176*(1), 151–162. https://doi.org/10.1016/j.jvolgeores.2008.07.007

Barbieri, R., Quirk, M. C., Frank, L. M., Wilson, M. A., & Brown, E. N. (2001). Construction and analysis of non-Poisson stimulus-response models of neural spiking activity. *Journal of Neuroscience Methods*, *105*(1), 25–37. https://doi.org/10.1016/S0165-0270(00)00344-7

Barbieri, R., Matten, E. C., Alabi, A. a, & Brown, E. N. (2005). A point-process model of human heartbeat intervals: new de nitions of heart rate and heart rate variability. *Am J Physiol Heart Circ Physiol*, *288*, 424–435. https://doi.org/10.1152/ajpheart.00482.2003.A

Bean, C. J., De Barros, L., Lokmer, I., Métaxian, J.-P., O'Brien, G. S., & Murphy, S. (2013). Long-period seismicity in the shallow volcanic edifice formed from slow-rupture earthquakes. *Nature Geoscience*, *7*(1), 71–75. https://doi.org/10.1038/ngeo2027

Bell, A. F., Hernandez, S., Gaunt, H. E., Mothes, P. A., Ruiz, M., Sierra, D., & Aguaiza, S. (2017). The rise and fall of periodic "drumbeat" seismicity at Tungurahua volcano, Ecuador. *Earth and Planetary Science Letters*, *475*, 58–70. https://doi.org/10.1016/j.epsl.2017.07.030

Bell, A. F., & Kilburn, C. R. J. (2012). Precursors to dyke-fed eruptions at basaltic volcanoes: Insights from patterns of volcano-tectonic seismicity at Kilauea volcano, Hawaii. *Bulletin of Volcanology*, *74*(2), 325–339. https://doi.org/10.1007/s00445-011-0519-3

Bell, A. F., & Kilburn, C. R. J. (2013). Trends in the aggregated rate of pre-eruptive volcano-tectonic seismicity at Kilauea volcano, Hawaii. *Bulletin of Volcanology*, *75*(1), 1–10. https://doi.org/10.1007/s00445-012-0677-y

Bell, A. F., Naylor, M., & Main, I. G. (2013). The limits of predictability of volcanic eruptions from accelerating rates of earthquakes. *Geophysical Journal International*, *194*(3), 1541–1553. https://doi.org/10.1093/gji/ggt191

Bell, A. F., Greenhough, J., Heap, M. J., & Main, I. G. (2011). Challenges for forecasting based on accelerating rates of earthquakes at volcanoes and laboratory analogues. *Geophysical Journal International*, *185*(2), 718–723. https://doi.org/10.1111/j.1365-246X.2011.04982.x

Bouchon, M., Karabulut, H., Aktar, M., Ozalaybey, S., Schmittbuhl, J., & Bouin, M.-P. (2011). Extended Nucleation of the 1999 Mw 7.6 Izmit Earthquake. *Science*, *331*(6019), 877–880. https://doi.org/10.1126/science.1197341

Boué, A., Lesage, P., Cortés, G., Valette, B., Reyes-Dávila, G. A., Arámbula-Mendoza, R., & Budi-Santoso, A. (2016). Performance of the "material Failure Forecast Method" in real-time situations: A Bayesian approach applied on effusive and explosive eruptions. *Journal of Volcanology and Geothermal Research*, *327*, 622–633. https://doi.org/10.1016/j.jvolgeores.2016.10.002

Boué, A., Lesage, P., Cortés, G., Valette, B., & Reyes-Dávila, G. A. (2015). Real-time eruption forecasting using the material Failure Forecast Method with a Bayesian approach. *Journal of Geophysical Research: Solid Earth*, *120*(4), 2143–2161.

https://doi.org/10.1002/2014JB011637
Buurman, H., West, M. E., & Thompson, G. (2013). The seismicity of the 2009 Redoubt eruption. *Journal of Volcanology and Geothermal Research*. https://doi.org/10.1016/j.jvolgeores.2012.04.024
Chouet, B. A., & Matoza, R. S. (2013). A multi-decadal view of seismic methods for detecting precursors of magma movement and eruption. *Journal of Volcanology and Geothermal Research*. https://doi.org/10.1016/j.jvolgeores.2012.11.013
Collombet, M. (2003). Seismicity rate before eruptions on Piton de la Fournaise volcano: Implications for eruption dynamics. *Geophysical Research Letters*, *30*(21), 1–5. https://doi.org/10.1029/2003GL017494
Gil-Cruz, F., & Chouet, B. a. (1997). Long-period events, the most characteristic seismicity accompanying the emplacement and extrusion of a lava dome in Galeras Volcano, Colombia, in 1991. *Journal of Volcanology and Geothermal Research*, *77*(1–4), 121–158. https://doi.org/10.1016/S0377-0273(96)00091-1
Green, D. N., & Neuberg, J. (2006). Waveform classification of volcanic low-frequency earthquake swarms and its implication at Soufrière Hills Volcano, Montserrat. *Journal of Volcanology and Geothermal Research*, *153*(1–2), 51–63. https://doi.org/10.1016/j.jvolgeores.2005.08.003
Hall, M. L., Steele, A. L., Bernard, B., Mothes, P. A., Vallejo, S. X., Douillet, G. A., … Ruiz, M. C. (2015). Sequential plug formation, disintegration by Vulcanian explosions, and the generation of granular Pyroclastic Density Currents at Tungurahua volcano (2013–2014), Ecuador. *Journal of Volcanology and Geothermal Research*, *306*, 90–103. https://doi.org/10.1016/j.jvolgeores.2015.09.009
Hidalgo, S., Battaglia, J., Arellano, S., Steele, A. L., Bernard, B., Bourquin, J., … Vásconez, F. (2015). SO2 degassing at Tungurahua volcano (Ecuador) between 2007 and 2013: Transition from continuous to episodic activity. *Journal of Volcanology and Geothermal Research*, *298*, 1–14. https://doi.org/10.1016/j.jvolgeores.2015.03.022
Holland, A., Watson, I. M., Phillips, J. C., Caricchi, L., & Dalton, M. P. (2011). Degassing processes during lava dome growth: Insights from Santiaguito lava dome, Guatemala. *Journal of Volcanology and Geothermal Research*, *202*(1–2), 153–166. https://doi.org/10.1016/j.jvolgeores.2011.02.004
Hotovec, A. J., Prejean, S. G., Vidale, J. E., & Gomberg, J. (2013). Strongly gliding harmonic tremor during the 2009 eruption of Redoubt Volcano. *Journal of Volcanology and Geothermal Research*, *259*, 89–99. https://doi.org/10.1016/j.jvolgeores.2012.01.001
Iverson, R. M., Dzurisin, D., Gardner, C. A., Gerlach, T. M., LaHusen, R. G., Lisowski, M., … Vallance, J. W. (2006). Dynamics of seismogenic volcanic extrusion at Mount St Helens in 2004-05. *Nature*, *444*(1), 439–443. https://doi.org/10.1038/nature05322
Johnson, J. B., Lees, J. M., Gerst, A., Sahagian, D., & Varley, N. (2008). Long-period earthquakes and co-eruptive dome inflation seen with particle image velocimetry. *Nature*, *456*(7220), 377–381. https://doi.org/10.1038/nature07429
Kilburn, C. R. J. (2003). Multiscale fracturing as a key to forecasting volcanic eruptions. *Journal of Volcanology and Geothermal Research*, *125*(3–4), 271–289. https://doi.org/10.1016/S0377-0273(03)00117-3
Kilburn, C. R. J. (2012). Precursory deformation and fracture before brittle rock failure and potential application to volcanic unrest. *Journal of Geophysical Research: Solid Earth*, *117*(B2), n/a-n/a. https://doi.org/10.1029/2011JB008703
Kilburn, C. R. J., & Voight, B. (1998). Slow rock fracture as eruption precursor at Soufriere Hills Volcano, Montserrat. *Geophysical Research Letters*, *25*(19), 3665. https://doi.org/10.1029/98GL01609
Krischer, L., Megies, T., Barsch, R., Beyreuther, M., Lecocq, T., Caudron, C., &

Wassermann, J. (2015). ObsPy: a bridge for seismology into the scientific Python ecosystem. *Computational Science & Discovery*, *8*(1), 14003. https://doi.org/10.1088/1749-4699/8/1/014003

De La Cruz-Reyna, S., & Reyes-Dávila, G. A. (2001). A model to describe precursory material-failure phenomena: Applications to short-term forecasting at Colima volcano, Mexico. *Bulletin of Volcanology*, *63*(5), 297–308. https://doi.org/10.1007/s004450100152

Lavallée, Y., Meredith, P. G., Dingwell, D. B., Hess, K.-U., Wassermann, J., Cordonnier, B., … Kruhl, J. H. (2008). Seismogenic lavas and explosive eruption forecasting. *Nature*, *453*(7194), 507–510. https://doi.org/10.1038/nature06980

Lensky, N. G., Sparks, R. S. J., Navon, O., & Lyakhovsky, V. (2008). Cyclic activity at Soufrière Hills Volcano, Montserrat: degassing-induced pressurization and stick-slip extrusion. *Geological Society, London, Special Publications*, *307*(1), 169–188. https://doi.org/10.1144/SP307.10

Linde, A. T., Agustsson, K., Sacks, I. S., & Stefansson, R. (1993). Mechanism of the 1991 eruption of Hekla from continuous borehole strain monitoring. *Nature*, *365*(6448), 737–740. https://doi.org/10.1038/365737a0

Lipovsky, B. P., & Dunham, E. M. (2015). Vibrational modes of hydraulic fractures: Inference of fracture geometry from resonant frequencies and attenuation. *Journal of Geophysical Research: Solid Earth*, *120*(2), 1080–1107. https://doi.org/10.1002/2014JB011286

Main, I. G. (1999). Applicability of time-to-failure analysis to accelerated strain before earthquakes and volcanic eruptions. *Geophysical Journal International*, *139*(3), F1–F6. https://doi.org/10.1046/j.1365-246x.1999.00004.x

McGuire, W., & Kilburn, C. R. J. (1997). Forecasting volcanic events: some contemporary issues. *Geologische Rundschau*, *86*, 439–445. https://doi.org/10.1007/s005310050152

McNutt, S. R. (2005). Volcanic Seismology. *Annual Review of Earth and Planetary Sciences*, *33*(1), 461–491. https://doi.org/10.1146/annurev.earth.33.092203.122459

Molina, I. (2004). Resonances of a volcanic conduit triggered by repetitive injections of an ash-laden gas. *Geophysical Research Letters*, *31*(3), L03603. https://doi.org/10.1029/2003GL018934

Neuberg, J., Collinson, A. S. D., Mothes, P. A., C. Ruiz, M., & Aguaiza, S. (2018). Understanding cyclic seismicity and ground deformation patterns at volcanoes: Intriguing lessons from Tungurahua volcano, Ecuador. *Earth and Planetary Science Letters*, *482*, 193–200. https://doi.org/10.1016/j.epsl.2017.10.050

Neuberg, J., Tuffen, H., Collier, L., Green, D., Powell, T., & Dingwell, D. (2006). The trigger mechanism of low-frequency earthquakes on Montserrat. *Journal of Volcanology and Geothermal Research*, *153*(1–2), 37–50. https://doi.org/10.1016/j.jvolgeores.2005.08.008

Neuberg, J., Luckett, R., Baptie, B., & Olsen, K. (2000). Models of tremor and low-frequency earthquake swarms on Montserrat. *Journal of Volcanology and Geothermal Research*, *101*(1–2), 83–104. https://doi.org/10.1016/S0377-0273(00)00169-4

Poli, P. (2017). Creep and slip: Seismic precursors to the Nuugaatsiaq landslide (Greenland). *Geophysical Research Letters*, *44*(17), 8832–8836. https://doi.org/10.1002/2017GL075039

Ramos, E. G., Hamburger, M. W., Pavlis, G. L., & Laguerta, E. P. (1999). The low-frequency earthquake swarms at Mount Pinatubo, Philippines: Implications for magma dynamics. *Journal of Volcanology and Geothermal Research*. https://doi.org/10.1016/S0377-0273(99)00091-8

Roberts, N. S., Bell, A. F., & Main, I. G. (2015). Are volcanic seismic b-values high, and if so when? *Journal of Volcanology and Geothermal Research*, *308*, 127–141. https://doi.org/10.1016/j.jvolgeores.2015.10.021

Robertson, R. M., & Kilburn, C. R. J. (2016). Deformation regime and long-term precursors to eruption at large calderas: Rabaul, Papua New Guinea. *Earth and Planetary Science Letters*, *438*(September 1994), 86–94. https://doi.org/10.1016/j.epsl.2016.01.003

Rodgers, M., Roman, D. C., Geirsson, H., LaFemina, P., Muñoz, A., Guzman, C., & Tenorio, V. (2013). Seismicity accompanying the 1999 eruptive episode at telica volcano, nicaragua. *Journal of Volcanology and Geothermal Research*, *265*, 39–51. https://doi.org/10.1016/j.jvolgeores.2013.08.010

Salvage, R. O., & Neuberg, J. (2016). Using a cross correlation technique to refine the accuracy of the Failure Forecast Method: Application to Soufrière Hills volcano, Montserrat. *Journal of Volcanology and Geothermal Research*, *324*, 118–133. https://doi.org/10.1016/j.jvolgeores.2016.05.011

Salvatier, J., Wiecki, T. V., & Fonnesbeck, C. (2016). Probabilistic programming in Python using PyMC3. *PeerJ Computer Science*, *2*, e55. https://doi.org/10.7717/peerj-cs.55

Shcherbakov, R., Yakovlev, G., Turcotte, D. L., & Rundle, J. B. (2005). Model for the Distribution of Aftershock Interoccurrence Times. *Physical Review Letters*, *95*(21), 218501. https://doi.org/10.1103/PhysRevLett.95.218501

Sigmundsson, F., Hooper, A., Hreinsdóttir, S., Vogfjörd, K. S., Ófeigsson, B. G., Heimisson, E. R., … Eibl, E. P. S. (2014). Segmented lateral dyke growth in a rifting event at Bárðarbunga volcanic system, Iceland. *Nature*, *517*(7533), 191–195. https://doi.org/10.1038/nature14111

Touati, S., Naylor, M., & Main, I. G. (2009). Origin and Nonuniversality of the Earthquake Interevent Time Distribution. *Physical Review Letters*, *102*(16), 168501. https://doi.org/10.1103/PhysRevLett.102.168501

Tuffen, H., & Dingwell, D. B. (2005). Fault textures in volcanic conduits: evidence for seismic trigger mechanisms during silicic eruptions. *Bulletin of Volcanology*, *67*(4), 370–387. https://doi.org/10.1007/s00445-004-0383-5

Tuffen, H., Dingwell, D. B., & Pinkerton, H. (2003). Repeated fracture and healing of silicic magma generate flow banding and earthquakes? *Geology*, *31*(12), 1089–1092. https://doi.org/10.1130/G19777.1

Tuffen, H., Smith, R., & Sammonds, P. R. (2008). Evidence for seismogenic fracture of silicic magma. *Nature*, *453*(7194), 511–514. https://doi.org/10.1038/nature06989

Vasseur, J., Wadsworth, F. B., Heap, M. J., Main, I. G., Lavallée, Y., & Dingwell, D. B. (2017). Does an inter-flaw length control the accuracy of rupture forecasting in geological materials? *Earth and Planetary Science Letters*, *475*(August), 181–189. https://doi.org/10.1016/j.epsl.2017.07.011

Voight, B. (1988). A method for prediction of volcanic eruptions. *Nature*, *332*(6160), 125–130. https://doi.org/10.1038/332125a0

Voight, B., & Cornelius, R. R. (1991). Prospects for eruption prediction in near real-time. *Nature*, *354*(APRIL 1991), 56–58. https://doi.org/10.1038/350695a0

White, R. A., Miller, A. D., Lynch, L., & Power, J. A. (1998). Observations of hybrid seismic events at Soufriere Hills Volcano, Montserrat: July 1995 to September 1996. *Geophysical Research Letters*, *25*(19), 3657–3660. https://doi.org/10.1029/98gl02427

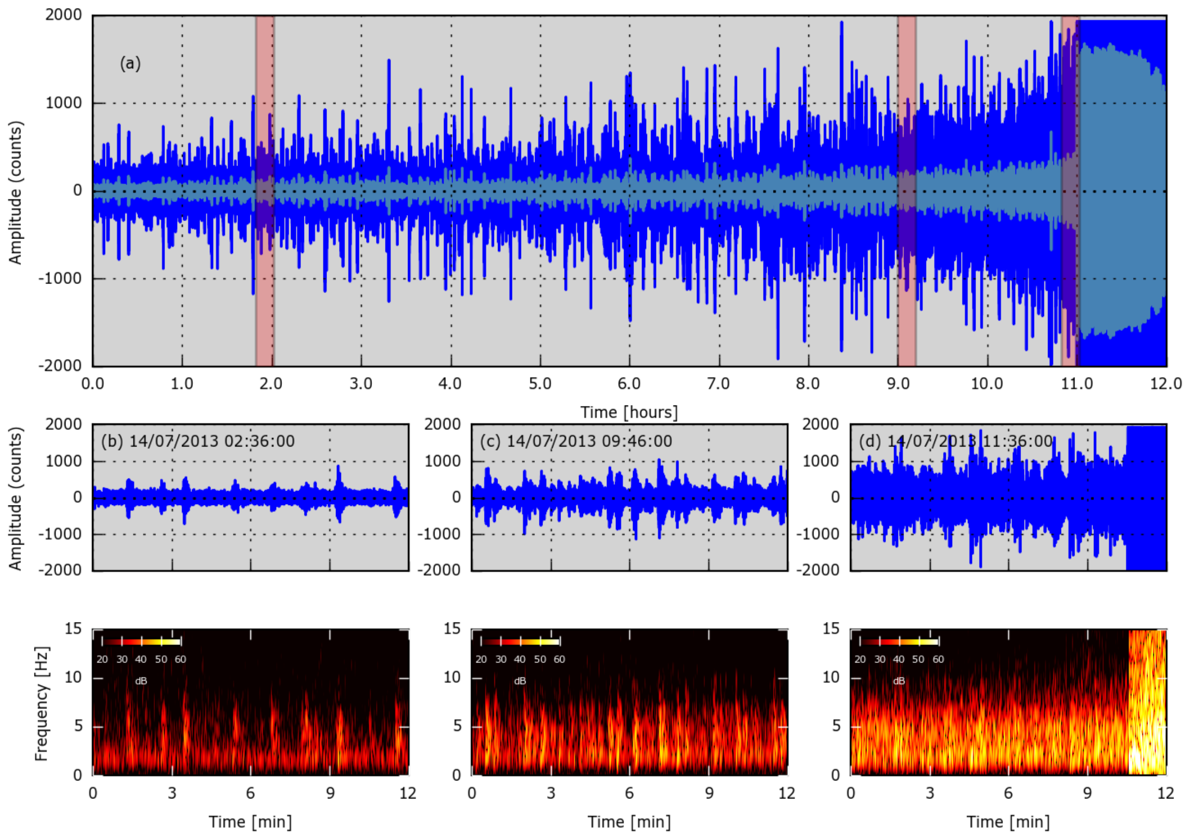

Figure 1: (a) Velocity time series for 12 hours of data recorded at RETU between 00:46 and 12:46 UTC on 14th July 2013, documenting the increase in earthquake rate and amplitude before the large explosion at 11:46. Dark blue line represents all data; light blue line represents data filtered between 0.1 and 8 Hz, and averaged over 10 seconds. (b)-(d) 12 minute times series and spectrograms for the intervals indicated by red bars in (a). Note quasi-periodic inter-event times and narrow range of earthquake amplitudes (b); progressive increase in earthquake rate and amplitude (c); and merger of earthquakes to form superficially continuous tremor immediately prior to eruption (d).

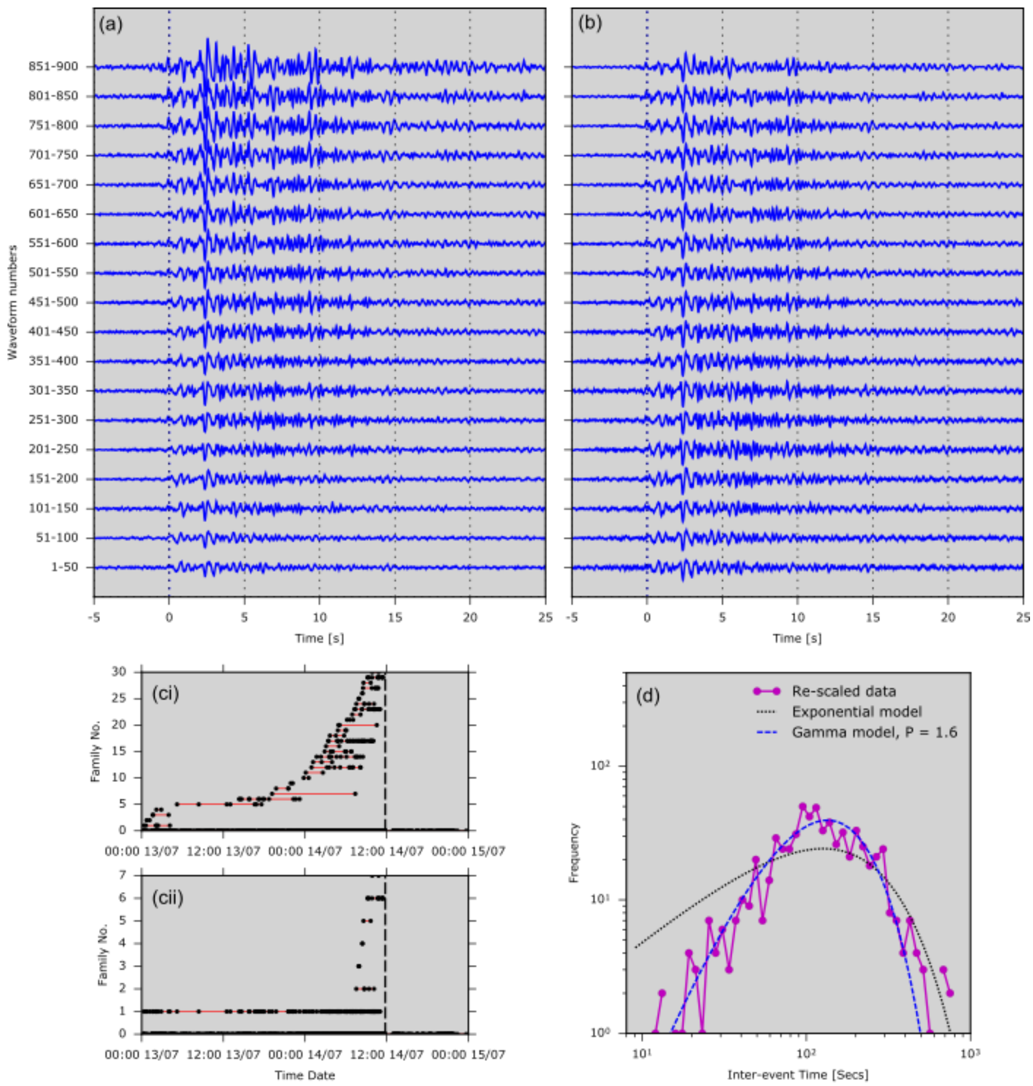

Figure 2: Top: Average waveform 'stacks' for 50 consecutive LP earthquakes recorded at RETU on 13 and 14 July 2013; (a) with original relative amplitudes preserved; (b) each stack normalized by amplitude to highlight waveform similarity. Bottom left: Families of similar earthquakes recorded at station RETU, 13-14 July 2013, determined using; (ci) single clustering stage based on cross-correlation threshold of 0.7; (cii) second additional cluster coalescence stage using cross-correlation threshold of 0.8. Black circles depict occurrence time of earthquakes belonging to different families. Red lines indicate temporal extent of each family. Family 0 consists of 'singleton' earthquakes that have no cross-correlations with other earthquakes above the 0.7 threshold. (d) Inter-event time distribution and best fitting models for re-scaled data for July 2013 pre-eruptive sequence. Data has been re-scaled according to equation (2) and mean posterior parameter values to account for increasing mean earthquake rate with time. Circles and solid lines represent actual data. Dotted black line shows best-fitting exponential inter-event time distribution model for the null hypothesis of a Poisson process for each phase (P=1). Dashed lines represent maximum-likelihood Gamma distributions with periodicity given by P value.

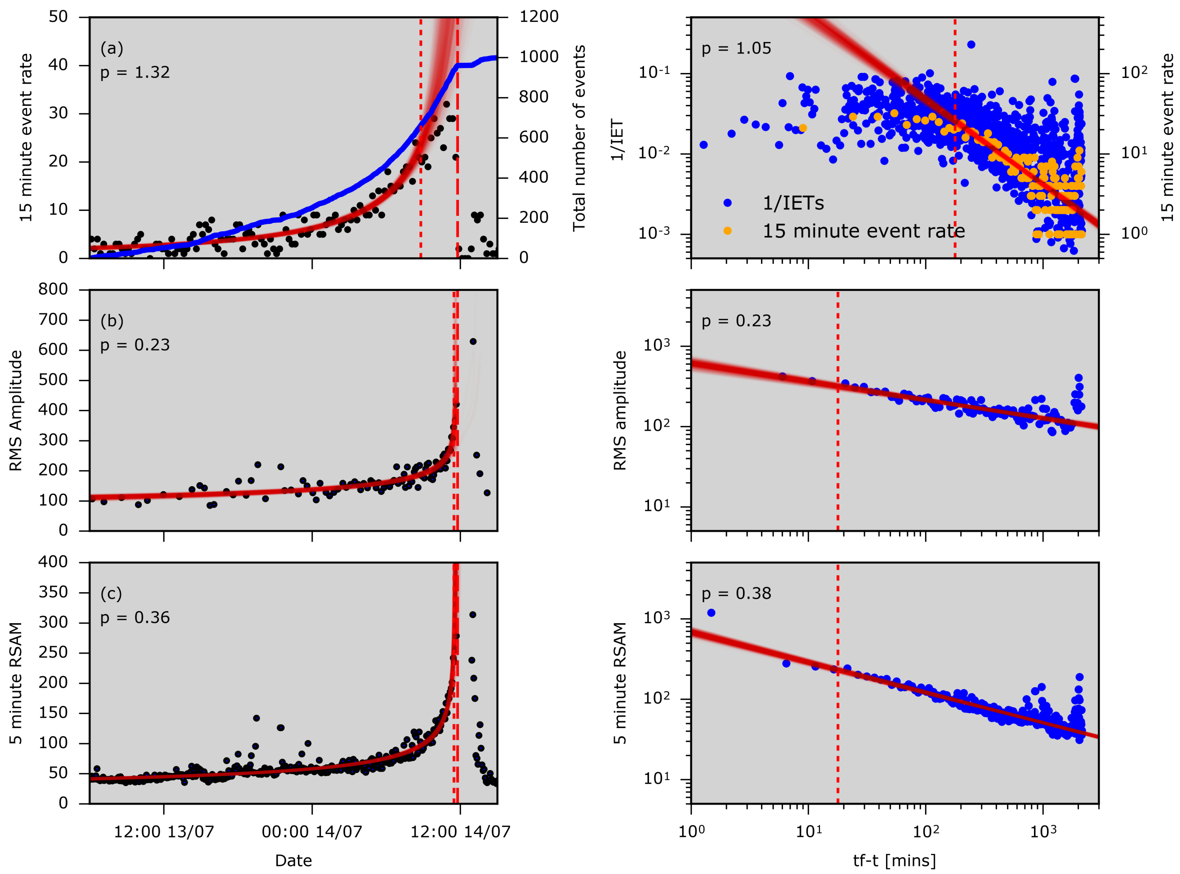

Figure 3: Linear time (left panels) and log-time from failure (right panels, i.e. 'time reversed') plots for (a) 15 minute earthquake rates and 1/(inter-event times), (b) mean 15 minute RMS earthquake amplitudes, and (c) mean 5 minute relative seismic amplitudes. In left panels, red curves show 500 'hind-cast' power-law models with parameter values (including eruption time) drawn from posterior distribution and corresponding mean hind-cast p-values. In right panels, red lines show 500 'retrospective' power-law posterior models, with eruption time known a priori, and corresponding mean retrospective p-values. In both instances, parameter posterior distributions are determined using data occuring before red dotted line. In (a) left panel, blue line represents total number of earthquakes. Note that the increase in earthquake rate slows towards eruption due to the merger of earthquakes (Fig. 1d), leading to a mismatch between model prediction and observations (a), and different mean power-law exponents and non-linearity for earthquake rates, amplitudes, and energy release rates.

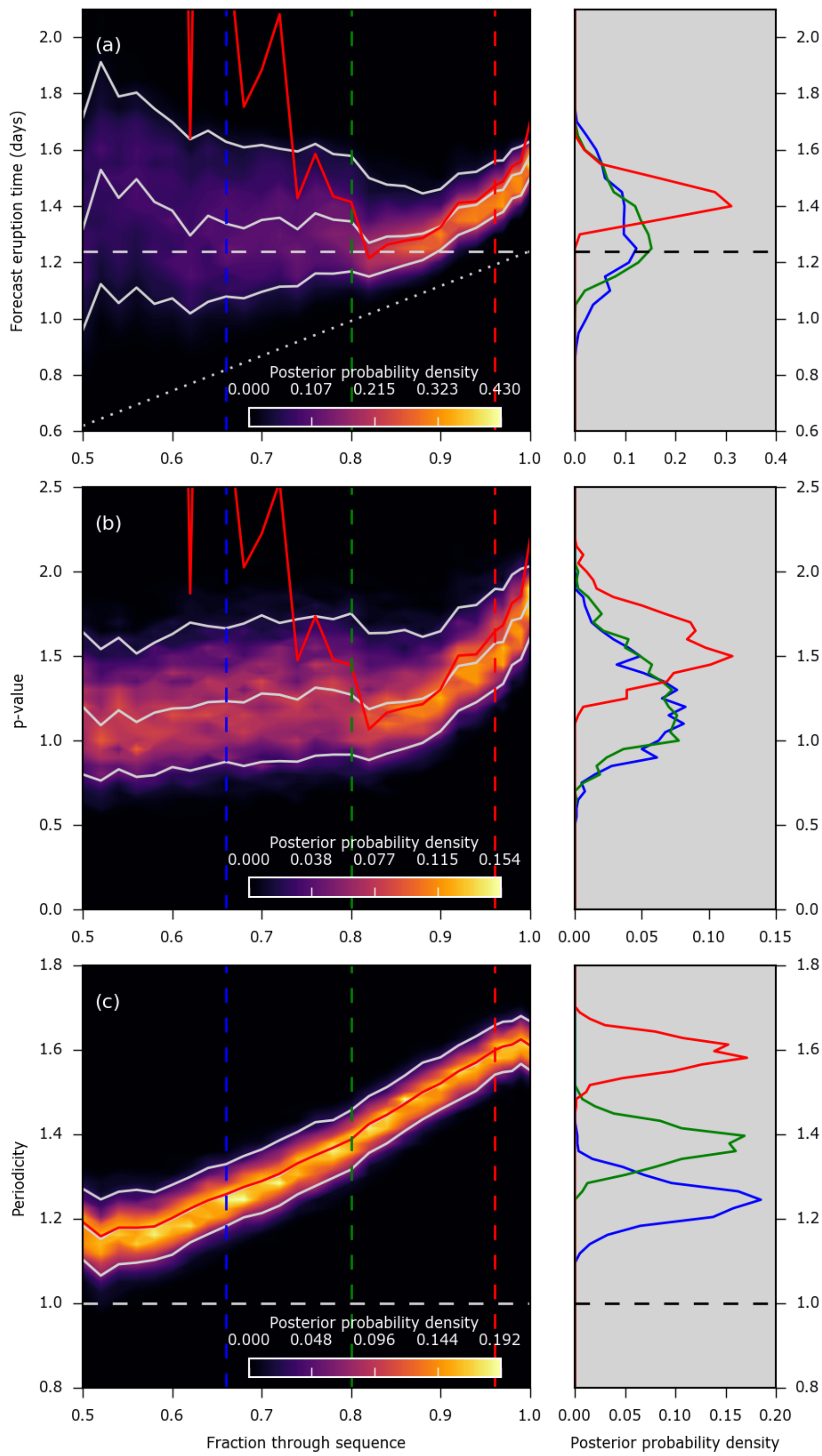

Figure 4: Left panels: Evolution of posterior distribution of (a) eruption time; (b) p-value; and (c) periodicity (mean inter-event time divided by its standard deviation, with horizontal dashed line representing a homogeneous Poisson process for reference), based on earthquake occurrence times. Colour scale indicateds the posterior probability density for parameters in a hindcast model, as determined incrementally through the sequence. White lines indicate the mean and 5% and 95% credibility intervals of the posterior. Solid red lines indicate maximum-likelihood estimates of power-law parameter values for an inhomogenous gamma

process. In (a), horizontal white dashed line indicates true value of eruption time, and dotted white line indicates actual time at which hindcast is made. Right panel: Posterior probability density distributions at times indicated by correspondingly coloured dashed lines in left panel (0.66, 0.8, and 0.96 of the sequence). Note increase in eruption time and p values estimates after 90% of the sequences due to rate saturation, and non-stationary increasing value of periodicity through the sequence.